Received 17 July 2008
Revised 1 November 2008
Accepted 15 December 2008

Convective heat transfer prediction for an axisymmetric jet impinging onto a flat plate with an improved k-ω model

S. Kubacki
Department of Flow, Heat and Combustion Mechanics, Ghent University, Ghent, Belgium and Institute of Thermal Machinery, Czestochowa University of Technology, Czestochowa, Poland, and
E. Dick
Department of Flow, Heat and Combustion Mechanics, Ghent University, Ghent, Belgium

Abstract

Purpose – This paper aims to provide improvements to the newest version of the k-ω turbulence model of Wilcox for convective heat transfer prediction in turbulent axisymmetric jets impinging onto a flat plate.

Design/methodology/approach – Improvements to the heat transfer prediction in the impingement zone are obtained using the stagnation flow parameter of Goldberg and the vortex stretching parameter of Wilcox. The third invariant of the strain rate tensor in the form of Shih *et al.* and the blending function of Menter are applied in order make negligible the influence of the impingement modifications in the benchmark flows for turbulence models. Further, it is demonstrated that for two-dimensional jets impinging onto a flat plate the stagnation region Nusselt number predicted by the original k-ω model is in good agreement with direct numerical simulation (DNS) and experimental data. Also for two-dimensional jets, the proposed modification is deactivated.

Findings – The proposed modification has been applied to improve the convective heat transfer predictions in the stagnation flow regions of axisymmetric jets impinging onto a flat plate with nozzle-plate distances H/D = 2, 6, 10 and Reynolds numbers Re = 23,000 and 70,000. Comparison of the predicted and experimental mean and fluctuating velocity profiles is performed. The heat transfer rates along a flat plate are compared to experimental data. Significant improvements are obtained with respect to the original k-ω model.

Originality/value – The proposed modification is simple and can be added to the k-ω model without causing stability problems in the computations.

Keywords Turbulence, Modelling, Heat transfer, Jets, Flow

Paper type Research paper

1. Introduction

Reynolds-averaged Navier-Stokes equations (RANS) models have great interest because of their low computational cost in resolving turbulent flows in many engineering applications, where a large eddy simulation (LES) method is too expensive. Among the RANS models, the eddy-viscosity models based on a linear relationship between the turbulent shear stress and the strain rate tensors are still very attractive due to their simplicity and robustness. On the other hand, RANS models based on this Boussinesq approximation have limitations, such as difficulties in prediction of boundary layer separation, secondary motion and turbulent production to dissipation rate in flow regions characterized by large level of strain. In the last few years some remedies have been proposed, leading to more reliable turbulent flow and convective heat transfer predictions and giving an impetus for their further validation in some challenging test cases.

International Journal of Numerical Methods for Heat & Fluid Flow
Vol. 19 No. 8, 2009
pp. 960-981

0961-5539
DOI 10.1108/09615530910994450

Among the eddy-viscosity models, the k-ω model of Wilcox (2006) has received great interest because of its usefulness in resolving turbulent flows near walls without requirement of wall damping functions. The reason for this favourable behaviour of the k-ω model is that extra dissipation is produced near walls compared to a k-ε model as a result of a so-called cross-diffusion term (Durbin, 1991). The cross-diffusion term appears when writing the k-ω model in the k-ε model formulation. Although this inherent property of the k-ω model poses advantages in resolving attached boundary layer flows and mildly separated flows, the accuracy of the earlier versions of the k-ω model was flawed by their sensitivity to the boundary conditions for the ω variable at the far-field boundaries, leading to ambiguous results in prediction of free shear flows. This drawback has been successfully removed in the present version of the k-ω model by careful addition of a cross-diffusion term in flow regions away from walls where the cross-diffusion term takes positive values.

Another important modification in the newest version of the k-ω model is the addition of a stress limiter. This limiter is applied in order to bound overprediction of the turbulent shear stress in flow regions characterized by large rates of strain, e.g. in stagnation flow regions. It should be mentioned that an analogous stress limiter has been applied in the shear stress transport (SST) model of Menter (1994). A similar remedy has been proposed by Durbin (1996) through realizability constraints. Such constraints can be imposed via modification of the turbulent time scale as it is done in the v^2-f model of Durbin (1991). As shown by Behnia *et al.* (1998), the v^2-f model significantly improves the heat transfer prediction in the stagnation flow region of an axisymmetric turbulent jet impinging onto a flat plate compared to a k-ε model by the cost of solving two additional equations: a transport equation for the velocity scalar v^2 and a Helmholtz equation for f. As a result, the v^2-f model is computationally more expensive than any one- or two-equation turbulence model. Further, it should be remarked that the boundary condition for f is a source of numerical stiffness and that, in order to improve convergence of the iterative process, the v^2- and f-equations should be solved as a coupled system so that the boundary condition for f can be treated implicitly (Durbin and Petterson Reif, 2001). Recently, the computational efficiency of the v^2-f model was improved by Laurence *et al.* (2004) and by Hanjalic *et al.* (2004) by redefinition of the velocity scale and by employing a different pressure-strain model in the f-equation.

It was demonstrated by Merci *et al.* (2004, 2005) that the influence of quadratic and cubic terms in the relation between Reynolds stresses and the velocity gradient has only negligible effect on the predicted heat transfer rate in an impingement region. Therefore, finally the constitutive relation was reduced to a first-order expression in their nonlinear turbulence viscosity model. The results obtained with the nonlinear k-ε model were similar to the results obtained with the v^2-f model. The results obtained by Merci *et al.* (2004, 2005) show the potential of adding sensors based on scalar invariants to the first order Boussinesq relation between the Reynolds stress tensor and the strain rate tensor. Jaramillo *et al.* (2007) showed that k-ω models perform much better than k-ε models in prediction of the heat transfer rates of jet flows impinging onto a flat plate. They also showed that inclusion of higher order terms in the constitutive law does not considerably improve the heat transfer predictions in stagnation flow regions. Successful implementation of a k-l eddy-viscosity model for prediction of impinging jet heat transfer has been obtained by Goldberg (2006) by modifying the eddy-viscosity formula with a sensor based on the difference between the magnitude of the shear rate and the magnitude of the rotation. So, the cited works suggest that also a k-ω model can be improved for prediction of the heat transfer in impinging jet flows by modifying the Boussinesq relation

between the Reynolds stress tensor and the strain rate tensor by taking into account sensors that detect impinging flow features.

In the present work, improvements have been obtained in prediction of the stagnation region Nusselt number of axisymmetric impinging jets using the k-ω turbulence model in the new version by Wilcox (2006) with a modification of the eddy viscosity expression based on the stagnation flow parameter of Goldberg (2006) and the vortex stretching parameter of Wilcox (2006). The first modification based on the Goldberg sensor has been introduced in order to prevent overprediction of the turbulent kinetic energy in the impingement point region. It is called here the stagnation flow correction. The second term based on the vortex stretching parameter has been introduced in order to suppress production of turbulent kinetic energy in the developing wall jet, underneath the deflected shear layer of the jet. It is called here the deflection region correction. The proposed modifications have been designed such that the results of simulations of free shear flows, channel and pipe flows and the flow over a backward facing step are not changed compared to the results of the basic k-ω model. This is crucial since the model coefficients and the constants in the auxiliary relations have been calibrated for these flows. The results for slot jets are also not modified by the proposed correction.

2. Model description

2.1 Transport equations

The transport equations of the k-ω (2006) model read:

$$\frac{D(\rho k)}{Dt} = P_k - \beta^* \rho k \omega + \frac{\partial}{\partial x_j}\left[\left(\mu + \sigma^* \rho \frac{k}{\omega}\right)\frac{\partial k}{\partial x_j}\right], \tag{1}$$

$$\frac{D(\rho \omega)}{Dt} = \alpha \frac{\omega}{k} P_k - \beta \rho \omega^2 + \frac{\partial}{\partial x_j}\left[\left(\mu + \sigma \rho \frac{k}{\omega}\right)\frac{\partial \omega}{\partial x_j}\right] + \rho \frac{\sigma_d}{\omega}\frac{\partial k}{\partial x_j}\frac{\partial \omega}{\partial x_j}, \tag{2}$$

with ρ the fluid density, μ the molecular viscosity, k the turbulent kinetic energy, ω the specific dissipation rate and $P_k = \tau_{ij}\partial U_i/\partial x_j$ with the components of the Reynolds stress tensor given by $\tau_{ij} = 2\mu_t S_{ij} - 2/3\rho k \delta_{ij}$. The turbulent viscosity is defined by:

$$\nu_t = \frac{k}{\tilde{\omega}}, \quad \tilde{\omega} = \max\left(\omega, C_{\lim}\sqrt{\frac{2S_{ij}S_{ij}}{\beta^*}}\right), \tag{3}$$

where $\beta^* = 0.09$, $C_{lim} = 7/8$ and S_{ij} are the components of rate of strain tensor. The remaining closure coefficients and some additional relations are:

$$\alpha = 13/25, \quad \beta = \beta_0 f_\beta, \quad \beta_0 = 0.0708, \quad \sigma = 0.5, \quad \sigma^* = 0.6, \quad \sigma_{do} = 0.125,$$

$$\sigma_d = \begin{cases} 0, & \dfrac{\partial k}{\partial x_j}\dfrac{\partial \omega}{\partial x_j} \le 0 \\ \sigma_{do} & \dfrac{\partial k}{\partial x_j}\dfrac{\partial \omega}{\partial x_j} > 0 \end{cases} \tag{4}$$

$$f_\beta = \frac{1+85\chi_\omega}{1+100\chi_\omega}, \quad \chi_\omega \equiv \left|\frac{\Omega_{ij}\Omega_{jk}S_{ki}}{\beta^*\omega^3}\right|,$$

where:

$$\Omega_{ij} = \frac{1}{2}\left(\frac{\partial U_i}{\partial x_j} - \frac{\partial U_j}{\partial x_i}\right), \quad S_{ij} = \frac{1}{2}\left(\frac{\partial U_i}{\partial x_j} + \frac{\partial U_j}{\partial x_i}\right). \tag{5}$$

One can see that a stress limiter is introduced in Equation (3) and that the sensitivity to free-stream values is limited by addition of a cross-diffusion term in the ω-equation (last term in Equation 2). Notice that the cross-diffusion term is only active away from the walls ($\sigma_d = \sigma_{do}$ in Equation 4) preserving the robustness and accuracy of the original k-ω model in the near wall region ($\sigma_d = 0$).

2.2 Proposed modification

A modification is proposed in the expression of the turbulent viscosity (3) by the introduction of an impingement function F_{imp} in order to suppress production of turbulent kinetic energy in flow regions deviating from simple shear:

$$\nu_t = \frac{k}{\tilde{\omega}}, \quad \tilde{\omega} = MAX\left(\omega, C_{\lim}F_{imp}\sqrt{\frac{2S_{ij}S_{ij}}{\beta^*}}\right) \tag{6}$$

The function F_{imp} is defined by:

$$F_{imp} = 1 + F_1(A + B) \tag{7}$$

The functions A and B read:

$$A = c_1|\tilde{W}||\tilde{S} - \tilde{\Omega}|\exp(-R_t/500) \tag{8}$$

$$B = c_2\hat{\chi}\exp(-R_t/200) \tag{9}$$

The F_1 term in Equation (7) is the blending function of Menter (1994):

$$F_1 = \tanh(\arg_1^4)$$

with:

$$\arg_1 = \min\left[\max\left(\frac{\sqrt{k}}{0.09\omega y}, \frac{500\mu}{\rho y^2\omega}\right), \frac{4\rho\sigma_{\omega 2}k}{CD_{SST}y^2}\right]$$

$$CD_{SST} = \max\left(2\rho\sigma_{\omega 2}\frac{1}{\omega}\frac{\partial k}{\partial x_i}\frac{\partial \omega}{\partial x_i}, 1.0e-20\right)$$

where $\sigma_{\omega 2} = 0.856$. The term arg_1 in the above formulation is based on the turbulent length scale $l_t = \sqrt{k}/(0.09\omega)$ normalized by the distance y to the nearest wall. The term l_t/y takes the value of about 2.5 in the logarithmic part of the boundary layer and it goes to zero in the outer flow regions. The other terms are safeguards ensuring that arg_1 does not go to zero in the viscous sublayer and takes a small value in the free stream, even for small free-stream values of ω. Here the F_1 function is used in order to deactivate the impingement correction (setting F_{imp} to unity) in free shear flows and in flows separating from a sharp corner. The constants c_1 and c_2 in Equations (8) and (9) were set to $c_1 = 2.5$ and $c_2 = 1.5$ and were determined by tuning them for two test cases in order to obtain good agreement in the predicted Nusselt number in the stagnation and flow deflection regions. The turbulent Reynolds number is defined by $R_t = k^2/(\varepsilon\nu) = k/(0.09\omega\nu)$. The critical values of the turbulent Reynolds number have been tuned for impinging jet flows.

The key factor in Equation (8) is the expression $|\tilde{S} - \tilde{\Omega}|$ which is used as a sensor for determination of flow regions strongly deviating from simple shear (Goldberg, 2006). The strain and vorticity invariants $\tilde{S}$ and $\tilde{\Omega}$ are given by:

$$\tilde{S} = \frac{1}{\beta^*\omega}\sqrt{2S_{ij}S_{ij}}, \tilde{\Omega} = \frac{1}{\beta^*\omega}\sqrt{2\Omega_{ij}\Omega_{ij}} \tag{10}$$

The sensor is used here following Goldberg who introduced it in a k-l model in order to reduce production of turbulent kinetic energy in stagnation and recirculation flows. For boundary layer flows $S \cong \Omega \cong \partial U/\partial y$ and therefore $|\tilde{S} - \tilde{\Omega}| \cong 0$ in simple shear flow, so that the correction term (8) is not active there. In stagnation flow regions, S is much higher than Ω and therefore the impingement function is larger than unity in Equation (7), providing damping of turbulent kinetic energy and reducing anomalous overprediction of the heat transfer rates. In order to deactivate the Goldberg sensor in other flows than stagnation flows, the F_1 function of Menter has been added in Equation (7) and the $|\tilde{W}|$ function of Shih *et al.* (1995) in Equation (8).

In order to leave the k-ω model predictions unmodified for the reference flows used to calibrate turbulence models, the $|\tilde{S} - \tilde{\Omega}|$ term is multiplied in Equation (8) by the third invariant of the strain rate tensor $|\tilde{W}|$:

$$|\tilde{W}| = \sqrt{6}|\min(0., W)|, \quad W = 2^{1.5}\frac{S_{ij}S_{jk}S_{ki}}{S^3} \tag{11}$$

The absolute value of W in Equation (11) is approximately equal to $|W| = 1/\sqrt{6}$ in axisymmetric expansion or contraction and it is zero for two-dimensional flows and pipe flows. Negative values of W are used in formula (11) to ensure that the activation of the Goldberg term is restricted to stagnation flow regions. The A term in Equation (7) controls the rate of damping of the turbulent kinetic energy in the stagnation flow region of an axisymmetric jet flow impinging onto a plate. As a result, more reliable impingement point heat transfer predictions can be achieved in flows characterized by weak turbulence production, which occurs when the plate is placed within the low shear core of the jet (at low nozzle-plate distances). At larger nozzle-plate distances, the low shear core of the jet starts to decay before the flow impingement due to turbulence diffusing from the edge towards the axis. For such cases, the stagnation flow correction introduced through the A term in Equation (8) should be less pronounced than for low nozzle plate distance. This effect is controlled by the turbulence Reynolds number. The

reduction of the turbulent viscosity by the impingement function F_{imp} becomes less with increasing turbulence Reynolds number.

On the other hand, as the width of the turbulent shear layer increases with downstream distance from the jet exit, it influences also the production of turbulent kinetic energy in the developing wall jet region. The turbulent flow undergoes strong deceleration in axial direction followed by acceleration in the direction parallel to the wall, and develops into a wall jet. This causes overprediction of the turbulent kinetic energy in the beginning of the developing wall jet. In order to produce more realistic predictions of turbulent kinetic energy in the boundary layer undergoing strong acceleration, the second term B has been added in Equation (7). The correction is provided via a modified form of the vortex-stretching parameter of Wilcox (2006):

$$\hat{\chi} = \frac{5\chi}{1+5\chi}, \quad \chi = \left| \frac{\Omega_{ij}\Omega_{jk}S_{ki}}{\beta^*\omega^3} \right| \tag{12}$$

The vortex-stretching parameter χ was introduced by Wilcox (2006) in the k-ω model in order to resolve the round-jet/plane-jet anomaly. The physical reasoning for introducing this term by Wilcox was that in an axisymmetric jet flow the vortex stretching mechanism is responsible for the transfer of energy from large to small eddies which causes increase of the dissipation rate of turbulent kinetic energy. In the present work, a similar sensor is used in order to limit overproduction of turbulent kinetic energy in the near wall region at larger distances from the symmetry axis, underneath the deflected shear layer of the jet. As shown by Wilcox, the parameter χ is zero for two-dimensional flows and fully developed pipe flow. Therefore the B term becomes negligible for the reference flows used in the calibration of the k-ω model. The constant 5 in Equation (12) was tuned for one of the test cases in order to obtain good correspondence between predicted and measured Nusselt number profiles in the developing wall-jet region. Similar to the A term, the B term has also a dependence on the turbulence Reynolds number.

3. Computational set-up

For most of the two-dimensional and axisymmetric jet flow simulations (free/impinging onto a flat plate), fully developed profiles were specified at the inlet of the computational domain which were separately computed assuming periodic boundary conditions. For some simulations, a flat profile is used. The inlet boundary was specified one nozzle width/diameter upstream of the jet exit. At the free stream inflow and at the far-field inflow boundaries turbulence intensity was set to $Tu = 0.001$ and the ratio of the turbulent to molecular viscosity was set to $\nu_t/\nu = 0.1$ in order to model the ambient conditions of the jets. At the outlet boundaries, zero normal derivative conditions were specified for k and ω. Figure 1 shows the computational domain for simulation of an axisymmetric jet impinging onto a flat plate.

For simulation of fully developed turbulent pipe-flow and 2D channel flow, the Reynolds numbers were specified at $Re_D = 40{,}000$ and $Re_H = 13{,}750$ (the Reynolds number is based on the average velocity and on pipe diameter and on channel height, respectively). For the flow past a backward-facing step, the inlet boundary conditions have been obtained from a precursor simulation of a developing 2D channel flow. The mean velocity and the turbulent quantities (k and ω) have been taken from the section where the predicted momentum thickness θ was equal to the experimentally measured value $Re_\theta = 5{,}000$. The inlet boundary conditions were specified, according to the

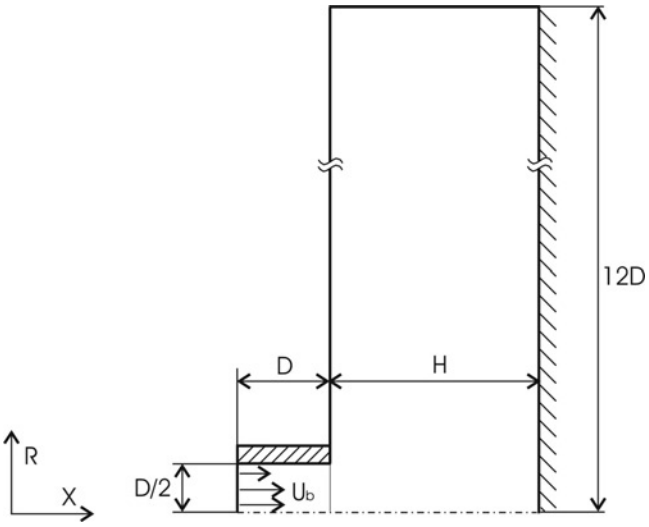

Figure 1.
Computational domain for impinging jet simulation

experimental data, four step heights upstream of the step. The pressure outlet boundary condition was applied at the exit from the computational domain located at the distance X/H = 50 (H is the height of the step).

The boundary conditions recommended by Menter (1994) have been specified at the no-slip walls for k and ω:

$$k = 0, \omega = 10\frac{6\nu}{\beta_1(\Delta y)^2} \tag{13}$$

where Δy is the first point away from the wall and $\beta_1 = 0.0708$.

The computations have been preformed with the Fluent code. The second order upwind scheme was applied for approximation of the convective terms in the momentum, energy, k- and ω-equations. The pressure staggering option (PRESTO) scheme has been applied for the pressure interpolation and the node-based approach was used for evaluation of the derivatives at the faces between cells. The semi implicit pressure linked equations (SIMPLE) algorithm was used for pressure-velocity coupling.

In all simulations structured grids have been applied. The nondimensional distance y^+ was less than 3 at all walls. For the axisymmetric jet flows impinging onto a flat plate, $y^+ < 0.5$ at the impingement plate. For impinging jet flow simulations the grid has been stretched close to the impingement plate, symmetry axis, jet exit and towards the edge of the nozzle (in the free shear layer). For the case H/D = 2 and Re = 23,000 the basic grid consists of 248 × 234 (axial or normal to the impingement plate x radial) points. Close to the impingement plate the first grid points were located at the axial distance 0.0002D. At the symmetry axis the smallest radial distance was equal to 0.005D. Towards the nozzle edge (in the free shear layer) the grid has been stretched in the radial direction with the smallest radial distance equal to 0.0008D. The stretching factor was not allowed to exceed 1.05. For higher nozzle-plate distances (H/D = 6 and 10) the number of grid points has been proportionally increased. For the other flows, basically the same strategy as described above has been applied in constructing the computational meshes.

In order to perform a grid-dependency study, two additional meshes have been constructed for the case H/D = 2, Re = 23,000. The coarse mesh consists of 132 × 234 points (note that the mesh has been coarsened in the axial direction) and the fine mesh consists of 496 × 468 points. Figure 2 shows the variation of the skin friction coefficient $c_f = \tau_w/(0.5\rho U_b^2)$, where τ_w is the wall shear stress $\tau_w = \mu(\partial V_r/\partial x)|_w$, U_b is the mean velocity at the jet exit and V_r is the radial velocity component) along the impingement plate obtained for simulation of an impinging jet flow on the coarse, basic and fine meshes. The c_f profiles obtained on the basic and fine meshes collapse, showing that for the mesh of 248 × 234 a grid-independent solution has been obtained. The grid of 132 × 234 points seems to be slightly too coarse as some deviations from the basic and fine grid solutions are observed at 1 < X/B < 3. Finally, the grid 248 × 234 has been used for further study of impinging jet flow at H/D = 2 and Re = 23,000.

4. Two-dimensional impinging jet flow results

Figure 3 shows the profiles of the Nusselt number computed by Hattori and Nagano (2004) using direct numerical simulation (DNS) and predicted by the k-ω model for simulation of a slot jet impinging onto a flat plate for Re = 4,500 with nozzle-plate distances H/B = 0.5 and H/B = 2. The Reynolds number is based on the slot width B and the mean velocity at the jet exit. The dotted line shows the heat transfer rate obtained for turbulent flow simulation but setting to zero the turbulent diffusivity in the energy equation. In the work of Hattori and Nagano (2004) a fully developed turbulent channel flow simulation was performed (using DNS) in order to provide the inlet conditions for the impinging jet flow simulations. Similarly, in the present computations, fully developed profiles, obtained from precursor computations of a channel flow using the k-ω model, of velocity, k and ω were prescribed at the nozzle exit. As shown in Figure 3 the stagnation point Nusselt number is well predicted using the k-ω model for both nozzle-plate distances. For H/B = 0.5 (Figure 3a) the stagnation

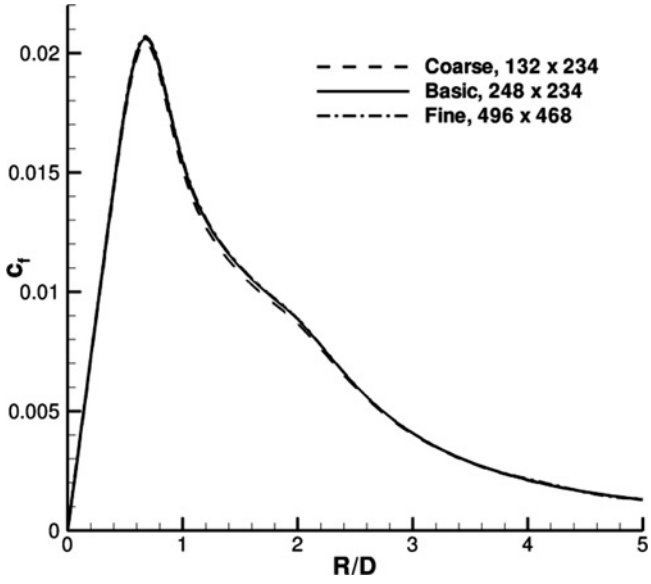

Figure 2.
Influence of the grid density on the skin friction coefficient along an impingement plate for simulation of impinging jet flow with H/D = 2 and Re = 23,000

point Nusselt number profile agrees quite well with the Nusselt number profile obtained by setting to zero the turbulent diffusivity in the energy equation. This result shows that for H/B = 0.5 the turbulent heat flux has negligible effect on the heat transfer in the stagnation flow region. The reason is that at impingement the low shear core of the jet formed at the nozzle exit still exits. In contrast, for H/B = 2 (Figure 3b), much higher differences are observed between the predicted heat transfer rates in the stagnation flow region using the k-ω model and the heat transfer rates obtained by setting to zero the turbulent diffusivity in the energy equation. This is due to increased contribution of the turbulent heat flux to the heat transfer in the stagnation flow region with increasing nozzle-plate distance as the low shear core of the jet disappears due to turbulent mixing. In both simulations, some differences are observed in the predicted heat transfer rate at larger distances from the symmetry line. For H/B = 0.5 (Figure 3a), the secondary peak in the Nusselt number profile is not predicted by the k-ω model. For H/B = 2 (Figure 3b), the heat transfer rates predicted by the k-ω model in the developing wall jet are lower than the heat transfer rates obtained by DNS. This is caused by relatively low production of turbulent kinetic energy in the near wall region of the developing wall jet predicted by the k-ω model.

Figure 4 shows the Nusselt number profile obtained for simulation of a slot jet impinging onto a flat plate for Re = 11,000 (based on the slot width B) with nozzle-plate distance H/B = 5. A flat velocity profile has been specified at the inlet to the computational domain with the turbulence intensity set to Tu = 0.025, according to the experimental data. The turbulent length scale has been set to $l_t = 0.015B$ (Jaramillo *et al.* 2008). Similarly to the previous results, the stagnation point heat transfer rate is well reproduced by the k-ω model. The dip in the Nusselt number profile (at X/B = 3) is not recovered by the simulation. The results of the predictions agree very well with the experimental data at larger distances from the symmetry line.

It should be remarked that some features like the secondary peak in the Nusselt number profile have been not reproduced in the present simulations. Nevertheless, the present version of the k-ω model has the ability of consistently reproducing the effect of the turbulent heat flux on the enhancement of the heat transfer in the stagnation flow region. The results show that there is no necessity of implementing further damping of the turbulent viscosity in the stagnation flow region for simulation of two-dimensional impinging jets. As shown in section 2.2 this was obtained by multiplying the A term

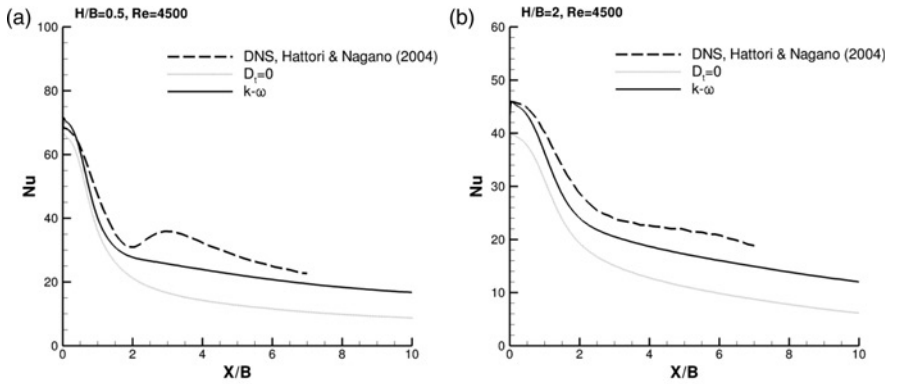

Notes: (a) H/B = 0.5; (b) H/B = 2
Source: Hattori and Nagano, 2004

Figure 3.
Nusselt number profiles along a flat plate computed by DNS and predicted by the k-ω model for simulation of a plane jet impinging onto a flat plate for Re = 4,500 and nozzle-plate distances

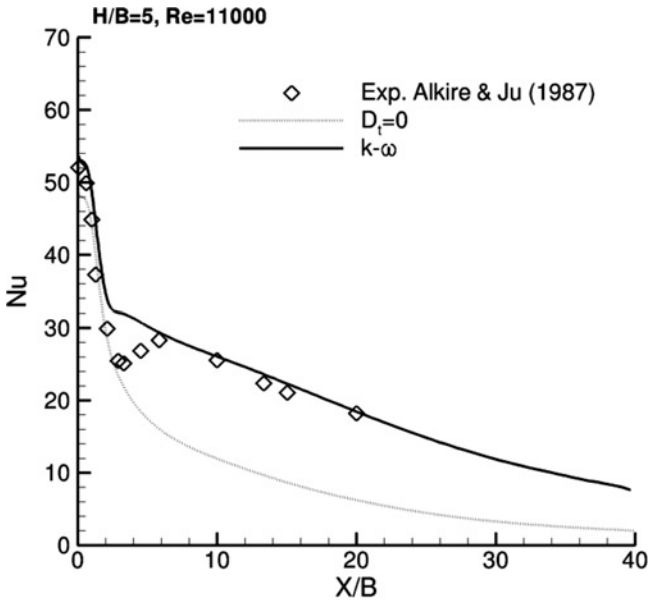

Figure 4.
Nusselt number profile along a flat plate for simulation of a slot impinging jet by the k-ω model compared with experimental data of Alkire and Ju (1987) for Re = 11,000 and H/B = 5

(Equation 8) by the term $|\tilde{W}|$ of Shih *et al.* (1995) and the B term (Equation 9) by a modified form of the vortex-stretching parameter $\hat{\chi}$ of Wilcox (2006).

5. Axisymmetric impinging jet flow results

The axisymmetric impinging jet flow configurations of Baughn and Shimizu (1989), Baughn *et al.* (1991) and Cooper *et al.* (1993) have been used for model tuning and model validation. The nozzle-plate distances are H/D = 2, 6 and 10. The inflow Reynolds numbers are 23,000 and 70,000 based on nozzle diameter and average velocity. The cases H/D = 2, Re = 23,000 and H/D = 6, Re = 70,000 were used for model tuning. The cases H/D = 2, Re = 70,000; H/D = 6, Re = 23,000 and H/D = 10, Re = 23,000 were used for model validation. We first illustrate the basic behaviour of the impingement and deflection sensors with the case H/D = 2 and Re = 23,000.

Figure 5a shows the contour plot of $|\tilde{S} - \tilde{\Omega}|$ for impinging jet flow simulation with H/D = 2 and Re = 23,000. The Goldberg sensor $|\tilde{S} - \tilde{\Omega}|$ is mainly active in the stagnation flow region and goes to small values farther away from the impingement zone. One should note that the Goldberg term is not active very close to the wall (for X/D > 1.99 and R/D < 1) where $S \cong \Omega$ and that some nonzero values of this parameter are obtained in other flow regions that deviate from simple shear flow. Figure 5b shows the impingement function F_{imp}. This function follows more-or less the behaviour of the Goldberg sensor, but its radial extension close to the plate is larger. This is due to the contribution of the deflection term given by Equation (9).

Figure 6 shows the contour plots of $F_1|\tilde{W}|$ and $F_1\hat{\chi}$ at two radial distances from the symmetry axis (close to R/D = 0 and 1). The $F_1|\tilde{W}|$ term attains unity at the symmetry axis and in the stagnation flow region and goes to lower values in the shear layer of the jet, as the flow is deflected in the radial direction (Figure 6c). Since this term multiplies the Goldberg term $|\tilde{S} - \tilde{\Omega}|$, it becomes clear that the A term given by Equation (8) is only active close to the symmetry axis and is reduced to very low values for R/D > 1.

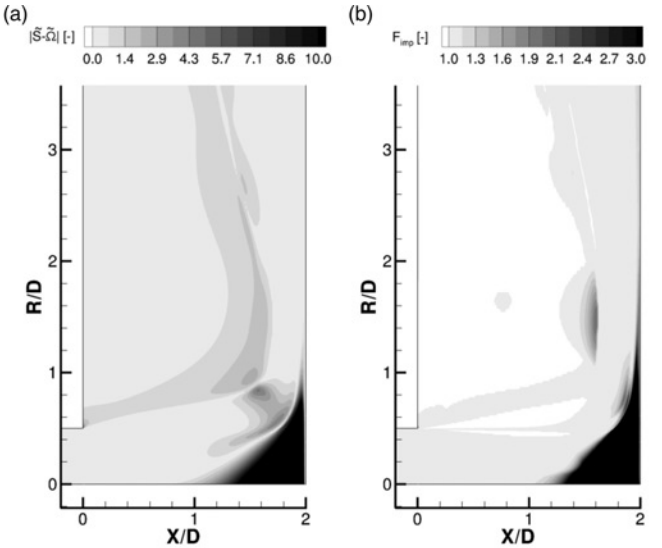

Figure 5.
Contour plots

Notes: (a) The Goldberg term |S – Ωl; (b) the impingement function F_{imp}

As mentioned above, the impingement function should also be active in the developing wall jet region (approx. at $1 < R/D < 2$) where the flow is strongly accelerated and then decelerated, causing overprediction of the turbulent length scale in the near-wall region. In order to reduce this anomaly, the B term has been added in Equation (7). Figures 6b and d show the contour plots of the $F_1\hat{\chi}$ parameter (which is used in the definition of the B term) at $R/D = 0$ and $R/D = 1$. The $F_1\hat{\chi}$ parameter is not equal to unity at the symmetry axis (on contrary to the $F_1|\tilde{W}|$ term). It switches to one at $R/D > 0.1$ and it stays also active for $X/D > 1.85$ at $R/D = 1$ (Figure 6d). It should be remarked that the $F_1\hat{\chi}$ term decays more slowly compared to the $F_1|\tilde{W}|$ term with increasing radial distance, but both terms do not modify the pure k-ω results in the fully developed wall jet. The impingement function F_{imp}, shown in Figure 5b, indicates the flow region where damping of the eddy viscosity is provided by Equation (6) if $F_{imp} > 1$. The impingement function is equal to unity in the shear layer of the jet as well as in the wall jet region at $R/D > 1.5$, so that the k-ω results are not modified there.

Figure 7 shows contour plots of turbulent kinetic energy obtained for simulation of the jet flow impinging onto a flat plate for $Re = 23{,}000$ at different nozzle-plate distances ($H/D = 2$, 6 and 10, corresponding to a, b and c). The results are obtained applying the proposed modification to the turbulent viscosity (Equation 6). As the jet exits the nozzle at $X/D = 0$ (see Figure 7a) it begins to spread and entrain ambient fluid. The shear layer of the jet initiated at the edge of the nozzle begins to develop. The flow is deflected in the radial direction in the stagnation flow region. Low levels of turbulent kinetic energy are predicted in the core of the jet until the flow reaches the plate while the maximum of the turbulent kinetic energy is located in the wall jet region at the distance $R/D \approx 2$. As it will be shown later, this agrees well with the experimental data. For higher nozzle-plate distance $H/D = 6$ (Figure 7b) also higher levels of turbulent kinetic energy are predicted in the stagnation flow region since the shear layer of the jet starts to penetrate to the core. The peak of turbulent kinetic

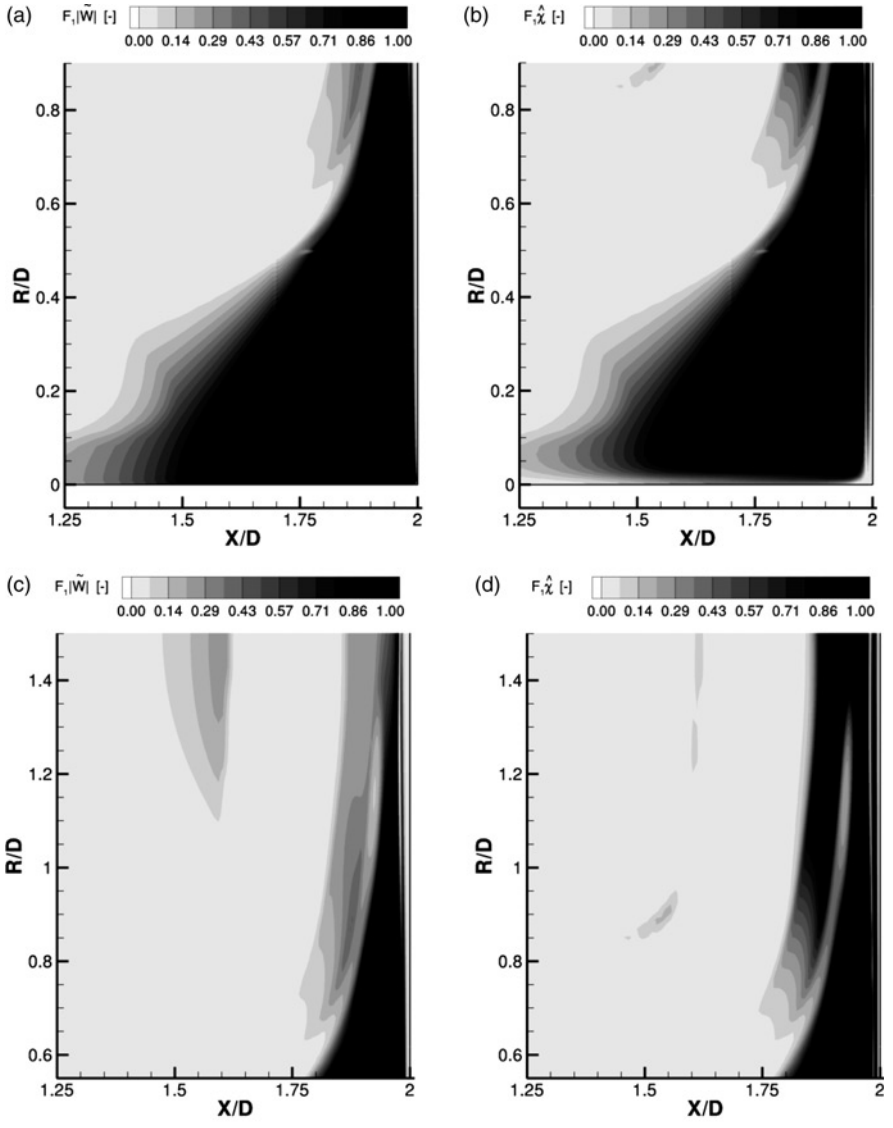

Notes: (a) and (b) close to the symmetry axis and (c) and (d) close to R/D = 1

Figure 6.
Contour plots of $F_1|\tilde{W}|$ (left) and $F_1\hat{\chi}$ (right) at different radial distances

energy is slightly shifted towards the symmetry axis (R/D $\approx$ 1.95) and a stronger spreading of turbulent kinetic energy is observed in the wall jet region compared to the nozzle-plate distance H/D = 2. As shown in Figure 7c much higher levels of turbulent kinetic energy are predicted in the stagnation flow region for the nozzle-plate distance H/D = 10, compared to the smaller distances, due to turbulence which already diffused to the jet axis. A slightly visible near-wall peak of turbulent kinetic energy is now located at R/D $\approx$ 1.2. Stronger spreading of turbulent kinetic energy is observed in the wall jet region compared to the lower nozzle-plate distances, H/D = 2 and H/D = 6.

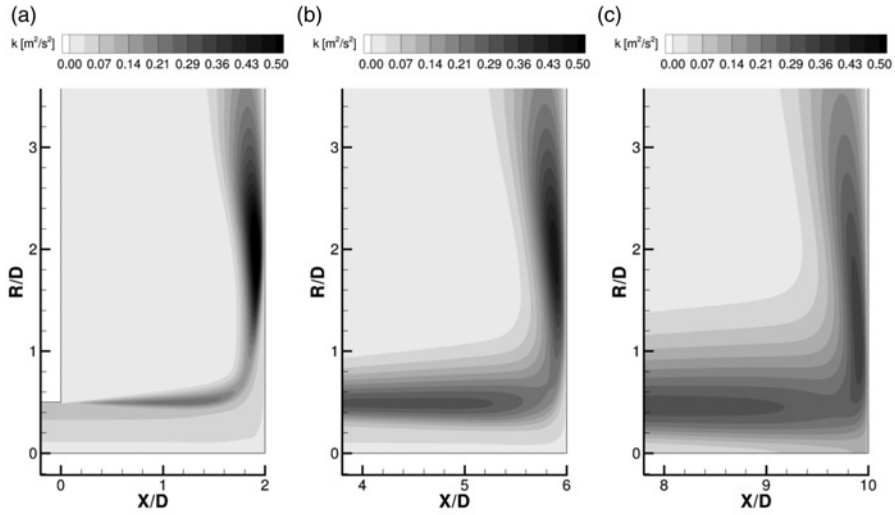

Figure 7.
Contour plots of turbulent kinetic energy close to the stagnation flow region for Re = 23,000 at different nozzle-plate distances

Notes: The results are obtained with the modified form of the turbulent viscosity (Equation 6) (a) H/D = 2, (b) H/D = 6 and (c) H/D = 10

Figure 8 shows the contour plots of specific dissipation rate ω in the stagnation flow regions (the same test cases as above). For small nozzle-plate distance H/D = 2 (Figure 8a) high values of ω are predicted in the shear layer initiated at the edge of the nozzle. Note that fully developed profiles were specified at the inlet to the computational domain located one jet diameter upstream of the jet exit. Since ω has high values at the wall (Equation 13), relatively high values of ω are also predicted in the developing shear layer of the jet, downstream from the edge of the pipe. This means that the

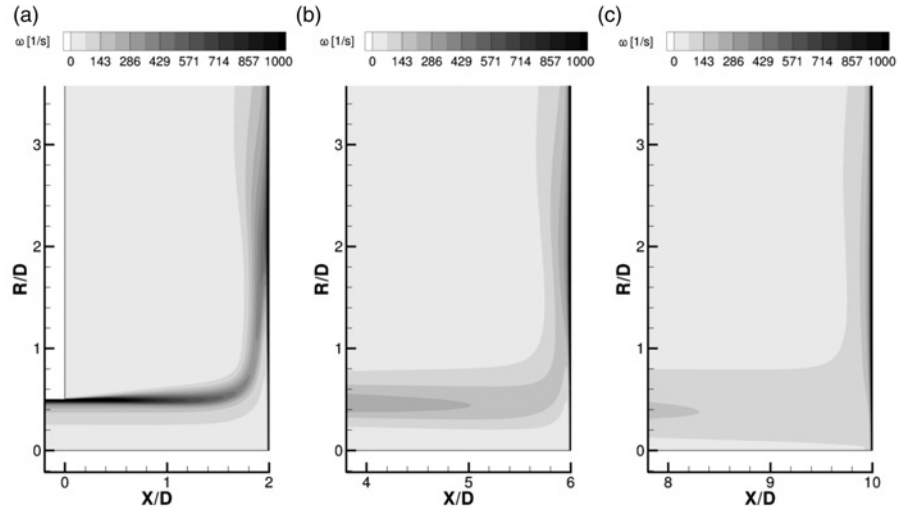

Figure 8.
Contour plots of specific dissipation rate close to the stagnation flow region for Re = 23,000 at different nozzle-plate distances

Notes: The results are obtained with the modified form of the turbulent viscosity (Equation 6); (a) H/D = 2, (b) H/D = 6 and (c) H/D = 10

turbulent length scales predicted in the shear layer of the jet are quite strongly affected by turbulent length scales predicted in the near-wall region of the nozzle and they influence also the turbulent length scales close to impingement plate. As the nozzle-plate distance is increasing (H/D = 6 Figure 8b and H/D = 10, Figure 8c) the specific dissipation rate ω becomes lower and lower in the stagnation flow region. This is due to reduction of the jet exit effect with increasing distance from the jet exit and subsequently larger turbulent length scales are able to penetrate towards the jet axis as a result of turbulent mixing in the shear layer of the jet (note that $\omega = \text{sqrt}(k)/(0.09*l_t)$, where l_t denotes turbulent length scale).

Figure 9 shows the contour plots of turbulent to molecular viscosity ratio (the same test cases as above). The plots clearly show the flow regions where damping of turbulent viscosity has been introduced in Equation (6) by the impingement function F_{imp} (Equation 7). Strong damping of turbulent kinetic energy in the impingement zone region is characterized by levels of $\nu_t/\nu = 10$ and lower. For low nozzle-plate distance H/D = 2 (left) the turbulent viscosity is damped stronger than for higher nozzle-plate distances. This is due to dependence of the damping terms A and B (in Equations 8 and 9, respectively) on the turbulence Reynolds number. As it will be shown later in the analysis of the heat transfer rates along the impingement plate such dependence is necessary in order to limit the suppression of the turbulent kinetic energy in the stagnation flow region with increasing nozzle-plate distance (in which case the flow becomes strongly affected by turbulence diffusing towards the jet axis).

Figure 10 shows the predicted and measured velocity magnitudes and fluctuating velocity components (radial and normal to the wall) at different radial positions, along lines perpendicular to the impingement plate for the nozzle-plate distance H/D = 2 and Re = 23,000. The data are normalized by the bulk velocity at the jet exit U_b and they are plotted as a function of dimensionless distance from the wall (H-x)/D, where H is the nozzle-plate distance and D is the nozzle diameter. The predicted mean and fluctuating velocity profiles are compared to the experimental data of Cooper *et al.* (1993). The solid

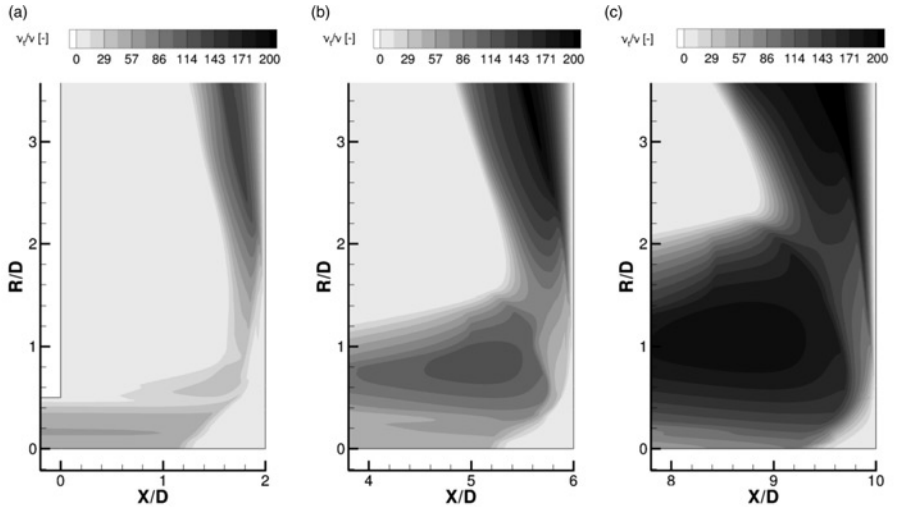

Notes: The results are obtained with the modified form of the turbulent viscosity (Equation 6); (a) H/D = 2, (b) H/D = 6 and (c) H/D = 10

Figure 9.
Contour plots of turbulent to molecular viscosity ratio close to the stagnation flow region for Re = 23,000 at different nozzle-plate distances

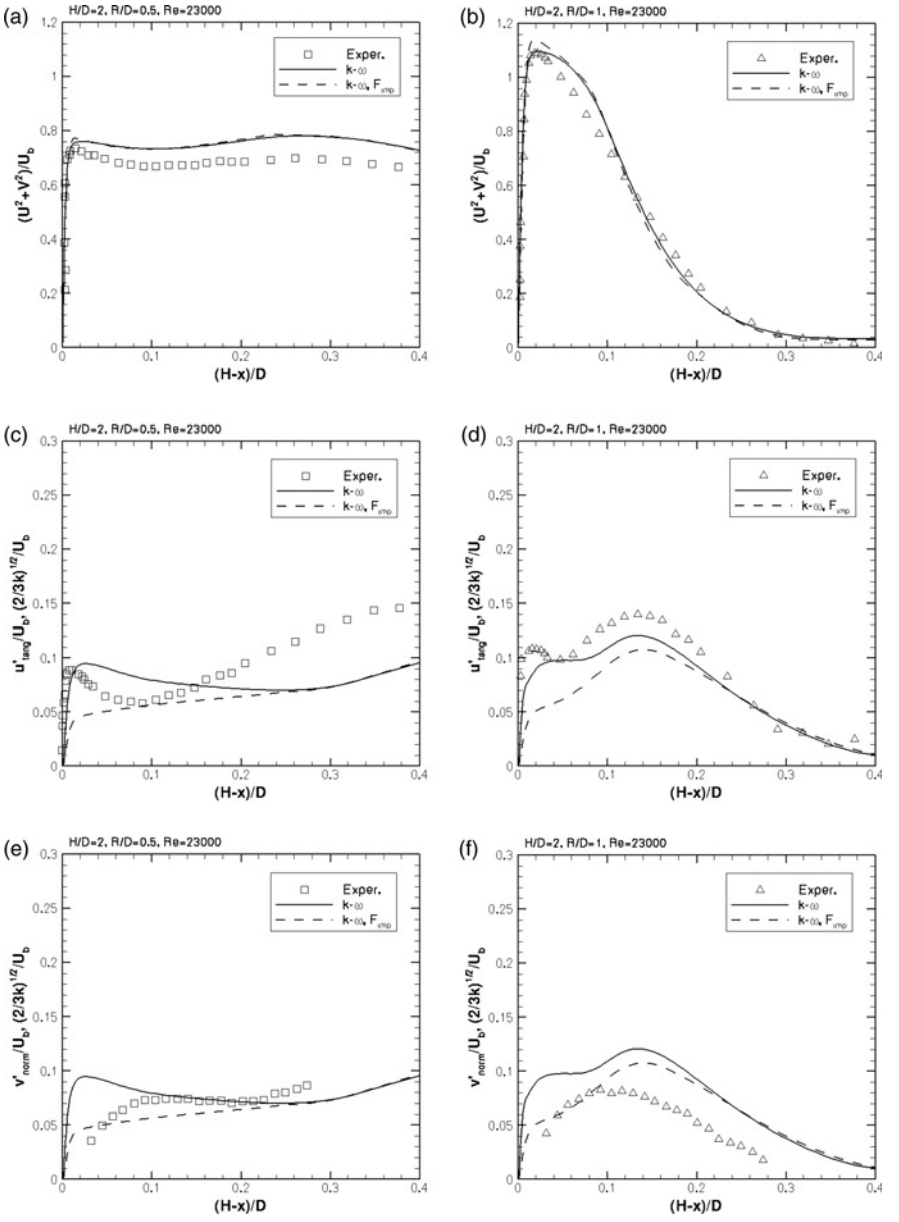

Figure 10.
Profiles of velocity magnitude (top) and fluctuating velocity components (radial – middle, normal to the wall -bottom) at the distance R/D = 0.5 (a, c and e), and R/D = 1 (b, d and f) from the symmetry axis for H/D = 2, Re = 23,000

lines represent the k-ω (2006) results while the dashed lines represent the results obtained with the k-ω model together with the proposed modifications. Both mean and fluctuating velocity profiles are well predicted close to the impingement point region (R/D = 0.5) using the k-ω (2006) model (Figures 10a, c and e). This is a consequence of limiting the turbulent shear stress in the stagnation flow region with the stress limiter. However, there is a slight overestimation of the turbulent kinetic energy. This overestimation is reduced by the proposed modification. Farther away from the symmetry axis at the

distance R/D = 1 (Figures 10b, d and f) the predicted fluctuating velocity components fall between the experimentally measured values of u'/U_b and v'/U_b for (H-x)/D < 0.2. Again, the slight overestimation of the turbulent kinetic energy is reduced by the proposed modification. Good agreement between predictions and measurements has also been obtained at larger distances from the symmetry axis and in the other test cases analyzed (for different values of the Reynolds number Re = 23,000, 70,000 and different nozzle-plate distances H/D = 2, 6; the results are not shown here).

One notices that close to the wall, the predicted fluctuating velocity (sqrt(2/3 k)) agrees better with the experimentally measured velocity component normal to the wall than with the radial one. This is wanted behaviour, which has been suggested by Durbin (1991). It forms the basis of the successful simulation of axisymmetric jet flows impinging onto a flat plate using the v^2-f model by Behnia *et al.* (1998), mentioned in the introduction. Since the wall normal fluctuating velocity components are more relevant to the heat transfer at the solid walls, it was of primary importance to mimic this behaviour with the proposed modifications of the k-ω model. In fact, the constants in the damping terms A and B (see Equations 8 and 9) have been determined in such a way that the predicted profiles of the fluctuating velocity component (sqrt(2/3 k)) agree better with the experimentally measured fluctuating velocity component normal to the wall than to the radial one, resulting in an improved heat transfer prediction in the stagnation flow region.

For the convective heat transfer simulation, the standard gradient hypothesis was applied. The turbulent heat flux vector is modelled by:

$$q_{Ti} = -\frac{\mu_t c_p}{\mathrm{Pr}_t}\frac{\partial T}{\partial x_i} \tag{14}$$

where c_p is the specific heat capacity at constant pressure and Pr_t is the turbulent Prandtl number ($Pr_t = 0.85$). The value of the molecular Prandtl number was set to Pr = 0.74. A constant value of temperature was specified at the impingement plate $T_w = 310K$ and in the nozzle flow $T_0 = 300K$. The local value of the Nusselt number was computed from:

$$Nu = \frac{D|\partial(T - T_0)/\partial n|_w}{T_w - T_0} \tag{15}$$

Figure 11a shows the predicted heat transfer rates along the impingement plate obtained with the k-ω model (solid line) and applying the k-ω model together with the proposed modification (dashed lines) for H/D = 2, Re = 23,000. The dotted line ($D_t = 0$) depicts the Nusselt number obtained for turbulent flow simulation using the original k-ω model and setting to zero the turbulent diffusivity in the energy equation. The predicted heat transfer rates are compared to the experimental data of Baughn and Shimizu (1989) and Baughn *et al.* (1991). The dotted line follows the experimental data up to the distance R/D = 1.2, which shows that in the stagnation flow region the heat transfer rates are mainly enhanced by turbulent shear stress which modifies the velocity gradient in vicinity of the surface and that the turbulent heat flux has only negligible effect on the energy transfer from the wall. The unmodified k-ω model overpredicts the Nusselt number at distance R/D < 1.2, which is caused by an overprediction of the turbulent kinetic energy in the stagnation flow region and the flow turning region due to the Boussinesq approximation. One should note that the shear stress correction which is already implemented in the new k-ω model reduces to some extend the turbulent kinetic energy in the stagnation flow region, but even

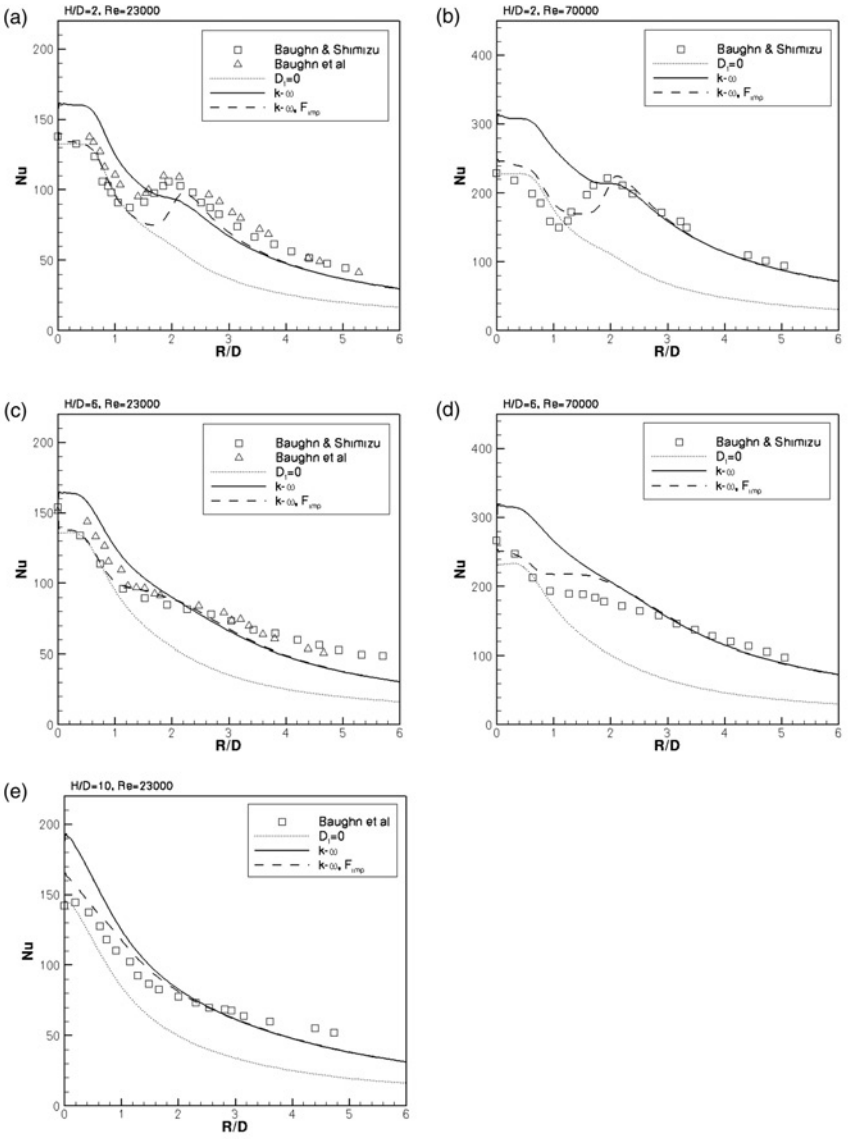

Figure 11.
Nusselt number distribution along a flat plate

Notes: The dotted line (Dt = 0) is obtained for turbulent flow simulation with the original k-ω model but setting to zero the turbulent diffusivity in the energy equation; (a) H/D = 2, Re = 23,000; (b) H/D = 2, Re = 70,000; (c) H/D = 6, Re = 23,000; (d) H/D = 6, Re = 70,000; (e) H/D = 10, Re = 23,000

stronger damping is necessary. The improved model (dashed line) shows much better correspondence between predictions and measurements in the stagnation flow region and flow turning region. This is a consequence of damping the turbulent viscosity by the impingement function F_{imp} in Equation (6). Further downstream (R/D > 1) the improved model predicts the second peak in the Nusselt number profile. The peak is

predicted a bit too far from the symmetry axis. As the flow develops into a wall jet, the heat transfer rates predicted by modified model collapse with the heat transfer rates predicted by the unmodified k-ω model.

Figure 11b shows the heat transfer rates predicted for H/D = 2, Re = 70,000. Similarly to the previous case, the stagnation point Nusselt number is substantially overpredicted by the original k-ω model and it is quite well recovered by adding the proposed modification to the turbulent viscosity. The experimental data shows a strong dip in the Nusselt number profile at R/D = 1, which is difficult to match correctly by the present turbulence model since the dotted line showing the heat transfer rate obtained with setting to zero the turbulent heat flux in the energy equation is already above the experimental data at R/D < 1. The second peak in the Nusselt number distribution (at R/D = 2) is well recovered by the improved model.

Figures 11c and d show the heat transfer rates predicted for the higher nozzle-plate distance H/D = 6 and Re = 23,000 and Re = 70,000, respectively. At this nozzle-plate distance the core of the jet starts to decay before the flow impingement. The experimentally measured heat transfer rates differ substantially from the previously analyzed heat transfer rates. Now, monotonic decay of the Nusselt number profiles is observed along the plate with increasing distance from the symmetry axis. For the low Reynolds number case (Re = 23,000) shown in Figure 11c, the original k-ω model slightly overpredicts the stagnation point heat transfer rate. The modified model slightly underestimates the Nusselt number at R/D = 0, while better agreement has been obtained between predicted and measured heat transfer rates at 0.5 < R/D < 2.5 compared to pure k-ω model. Further downstream, in the wall jet region, the heat transfer rates predicted by the modified and the original k-ω models are close to each other. For the higher Reynolds number case (H/D = 6, Re = 70,000) shown in Figure 11d, the differences between predictions by the original k-ω model and the measurements are much higher. The stagnation point Nusselt number predicted by the modified k-ω model is in good agreement with the experimental data and also the monotonic decay of the heat transfer rate with increasing distance from the symmetry axis is well reproduced by the predictions. It should be stressed that for this case both the A and B terms in Equation (7) play an important role in reducing the near-wall production of turbulent kinetic energy. The A term (Equation 8) reduces the level of turbulence kinetic energy in the impingement point region (R/D < 0.5) where the B term (Equation 9) prevents overprediction due to flow deflection (R/D > 0.5).

For the last test case analysed (H/D = 10, Re = 23,000), shown in Figure 11e, the core of the jet already has decayed before the flow impingement. This causes intensification of turbulence mixing in the impingement zone, which can be deduced by the quite strong differences in the variation of the dotted line with respect to the experimental data at R/D > 0.2 and by strong decrease of the heat transfer rates with increasing distance from the symmetry axis. Again, the original k-ω model overpredicts the stagnation point Nusselt number while the modified model provides much better agreement between predictions and measurements.

6. Verification of the calibration flows for turbulence models

We verify that the proposed modification to the k-ω model does not alter the solution of the flows that have been used for calibration of the basic model (Wilcox, 2006): free plane and axisymmetric jet flows, pipe and channel flows and flow over a backward facing step.

Figure 12 shows the mean velocity and the turbulent kinetic energy profiles for simulation of a two-dimensional jet flow along X/Y (where X- and Y- denote the

spanwise and streamwise coordinates) predicted by the k-ω model (solid line) and applying the k-ω model together with the proposed modification (dashed line). The flow properties are analyzed at the dimensionless distance Y/B = 5 from the nozzle exit. As shown, the predictions obtained using the impingement detector almost collapse with the results obtained using the original k-ω model. It should be remarked that a fully developed turbulent profile was specified at the inlet of the computational domain (specified one slot width upstream of the jet exit) in order to verify whether the proposed near-wall modifications would be activated there. As shown, this is not the case. Further downstream from the jet exit (in the self-similar region) the mean and fluctuating velocity profiles are also not modified (results not shown here).

The results of the simulation of an axisymmetric jet flow (Figure 13) show that the predicted mean velocity and turbulent kinetic energy profiles are also not modified along Y/X (where Y- and X- denote the radial and axial coordinates, respectively) when the proposed modification is applied.

Figure 14 shows the mean velocity and turbulent kinetic energy profiles (the former normalized by velocity at the symmetry axis, the latter normalized by friction velocity u_τ) for pipe-flow simulation using the k-ω model (solid line) and applying the k-ω model together with the proposed modification (dashed line). The proposed modifications do

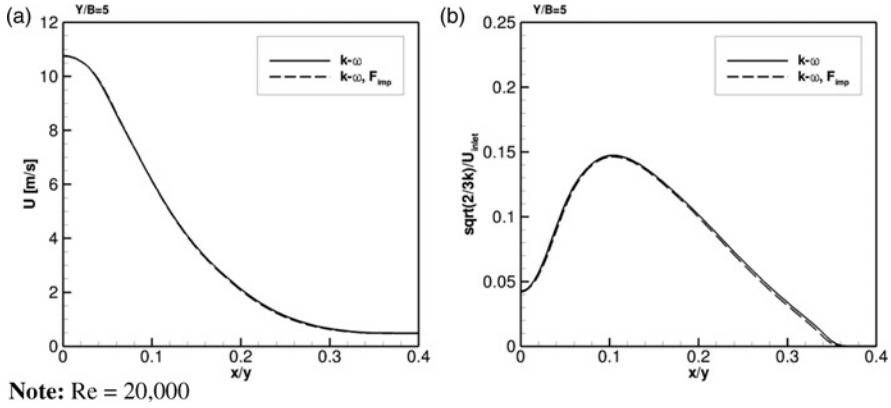

Figure 12.
Comparison of predicted (a) mean velocity and (b) turbulent kinetic energy profiles for simulation of the plane jet at distance Y/B = 5 from the jet exit

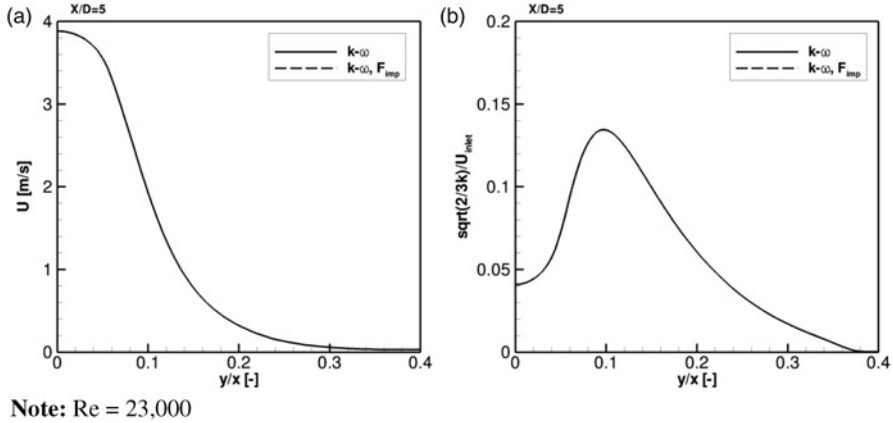

Figure 13.
Comparison of predicted (a) mean velocity and (b) turbulent kinetic energy profiles for simulation of the axisymmetric jet flow at distance X/D = 5 from the jet exit

not change the k-ω results for the pipe-flow simulation. As shown by Wilcox (2006), the peak value of k near the wall is not correctly captured by the k-ω model, but the Reynolds shear stress profile corresponds well to the experimental data of Laufer (1952).

A similar conclusion can be drawn from Figure 15 showing the predicted mean velocity and turbulent kinetic energy profiles (the former normalized by velocity at the symmetry line, the latter normalized by friction velocity u_τ) in the flow through the channel compared with computed results from DNS (DNS results of Mansour *et al.* (1988)). The proposed modification does not change the standard k-ω model predictions for the 2D channel flow. Similarly, as for the pipe-flow simulation, the peak value of k near the channel wall is not well predicted by the k-ω model, but the turbulent shear stress is in much better agreement with DNS results (results not shown here).

As a last example, the predicted skin friction coefficient c_f is shown in Figure 16 for simulation of the flow over a backward facing step using the k-ω model (solid line) and applying the proposed modification (dashed line). The results of the simulations are compared with the experimental data of Driver and Seegmiller (1985). In the present simulations, using the k-ω model the reattachment is predicted at 6.88 step heights downstream of the step. The same result is obtained using the k-ω model and applying

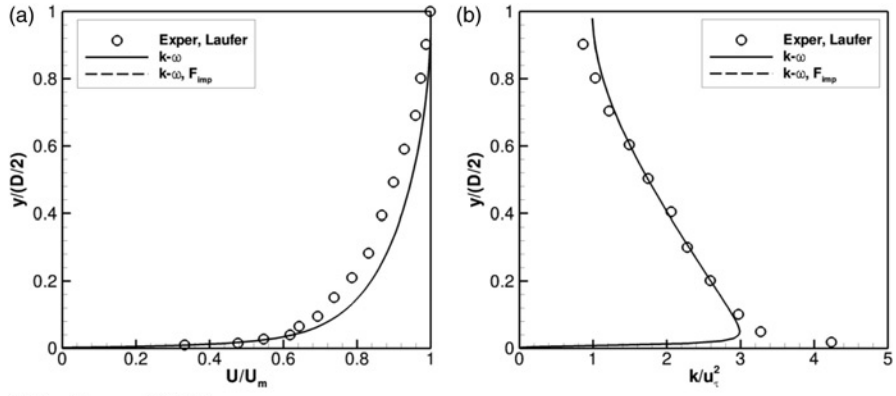

Figure 14.
Comparison of computed and measured (a) mean velocity and (b) turbulent kinetic energy profiles for flow in a pipe

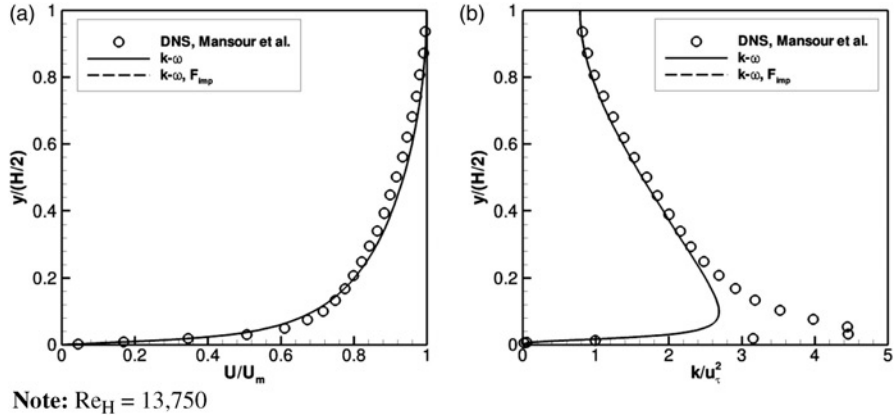

Figure 15.
Comparison of predicted by turbulence model and computed using DNS (a) mean velocity and (b) turbulent kinetic energy profiles for two-dimensional channel flow simulation

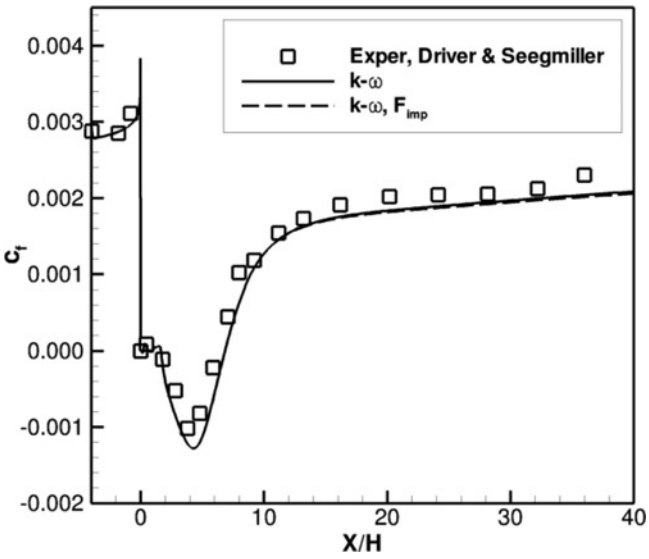

Figure 16.
Computed and measured skin friction coefficient for the flow over a backward facing step, $Re_\theta = 5{,}000$

the modification based on the impingement detector. This is within 10 per cent of the measured value 6.26H (where H is the step height). This example shows that the k-ω model provides reliable results for prediction of the flow separating from sharp corner. Further adjustment of the k-ω model for such flows is not necessary.

7. Summary

Improved stagnation point heat transfer predictions have been obtained for simulation of axisymmetric jet flows impinging onto a flat plate when a modification to the eddy viscosity formula based on an impingement function has been applied to the k-ω model in order to suppress production of turbulent kinetic energy in the stagnation and flow deflection regions. Verification of the proposed modification has been performed for simulation of free shear flows, channel and pipe flows, the flow over a backward facing step and slot jets impinging onto a flat plate, which shows that the proposed modification does not alter the k-ω model predictions in these reference flows. The proposed modification does not lead to stability problems in the flow regions characterized by large levels of strain, and the robustness of the k-ω model is preserved.

References

Alkire, R. and Ju, J. (1987), "High speed selective electroplating with impinging two-dimensional slot jet flow", *Journal of the Electrochemical Society*, Vol. 134 No. 2, pp. 294-9.

Baughn, J.W. and Shimizu, S. (1989), "Heat transfer measurements from a surface with uniform heat flux and an impinging jet", *Journal of Heat Transfer*, Vol. 111 No. 4, pp. 1096-8.

Baughn, J.W., Hechanova, A.E. and Yan, X. (1991), "An experimental study of entrainment effects on the heat transfer from a flat surface to a heated circular impinging jet", *Journal of Heat Transfer*, Vol. 113 No. 4, pp. 1023-5.

Behnia, M., Parneix, S. and Durbin, P.A. (1998), "Prediction of heat transfer in an axisymmetric jet impinging on a flat plate", *International Journal of Heat and Mass Transfer*, Vol. 41 No. 12, pp. 1845-55.

Cooper, D., Jackson, D.C., Launder, B.E. and Liao, G.X. (1993), "Impinging jet studies for turbulence model assessment-I. Flow-field experiments", *International Journal of Heat and Mass Transfer*, Vol. 36 No. 10, pp. 2675-84.

Driver, D.M. and Seegmiller, H.L. (1985), "Features of reattaching turbulent shear layer in divergent channel flow", *AIAA Journal*, Vol. 23 No. 1, pp. 163-71.

Durbin, P.A. (1991), "Near-wall turbulence closure without damping functions", *Theoretical and Computational Fluid Dynamics*, Vol. 3 No. 1, pp. 1-9.

Durbin, P.A. (1996), "On the k-ε stagnation point anomaly", *International Journal of Heat Fluid Flow*, Vol. 17, pp. 89-90.

Durbin, P.A. and Pettersson Reif, B.A. (2001), *Statistical Theory and Modelling for Turbulent Flows*, John Wiley & Sons, New York, NY.

Goldberg, U. (2006), "A k-l turbulence closure sensitized to non-simple shear flows", *International Journal of Computational Fluid Dynamics*, Vol. 20 No. 9, pp. 651-6.

Hanjalic, K., Popovac, M. and Hadziabdic, M. (2004), "A robust near-wall elliptic-relaxation eddy-viscosity turbulence model for CFD", *International Journal of Heat and Fluid Flow*, Vol. 25 No. 6, pp. 1047–51.

Hattori, H. and Nagano, Y. (2004), "Direct numerical simulation of turbulent heat transfer in plane impinging jet", *International Journal of Heat and Fluid Flow*, Vol. 25, pp. 749-58.

Jaramillo, J.E., Perez-Segarra, C.D., Oliva, A. and Claramunt, K. (2007), "Analysis of different RANS models applied to turbulent forced convection", *International Journal of Heat and Mass Transfer*, Vol. 50 Nos 19/20, pp. 3749-66.

Jaramillo, J.E., Perez-Segarra, C.D., Rodriguez, I. and Oliva, A. (2008), "Numerical study of plane and round impinging jets using RANS models", *Numerical Heat Transfer, Part B*, Vol. 54, pp. 213-37.

Laufer, J. (1952), *The Structure of Turbulence in Fully Developed Pipe Flow*, NACA Report No. 1174.

Laurence, D.R., Uribe, J.C. and Utyuzhnikov S.V. (2004), "A robust formulation of the v2–f model", *Flow, Turbulence and Combustion*, Vol. 73, pp. 169-85.

Mansour, N.N., Kim, J. and Moin, P. (1988), "Reynolds stress and dissipation rate budgets in turbulent channel flow", *Journal of Fluid Mechanics*, Vol. 194, pp. 15-44.

Menter, F.R. (1994), "Two-equation eddy-viscosity turbulence models for engineering applications", *AIAA Journal*, Vol. 32 No. 8, pp. 1598-605.

Merci, B., Van Maele, K. and Dick, E. (2005), "Impingement heat transfer with a nonlinear first-order k-ε model", *Journal of Thermophysics and Heat Transfer*, Vol. 20 No. 1, pp. 144-8.

Merci, B., De Langhe, C., Lodefier, K. and Dick, E. (2004), "Axisymmetric impingement heat transfer with a nonlinear k-ε model", *Journal of Thermophysics and Heat Transfer*, Vol. 18 No. 1, pp. 100-7.

Shih, T.H., Liou, W.W., Shabbir, A., Yang, Z., and Zhu, J. (1995), "A new k-ε eddy viscosity model for high Reynolds number turbulent flows", *Computational Fluids*, Vol. 23 No. 3, pp. 227-38.

Wilcox, D.C. (2006), *Turbulence Modeling for CFD*, DCW Industries, La Cañada, Flintridge.

Corresponding author
Erik Dick can be contacted at: Erik.Dick@UGent.be